Numerical Solution of Two- and Three-Dimensional Rotor Tip Leakage Models

A. R. Wadia*
General Motors Corporation, Indianapolis, Indiana

Blade tip losses represent a major efficiency penalty in a turbine or compressor rotor. These losses are presently controlled by maintaining close tolerances on tip clearances. This paper initially focuses on the control of tip leakage flow through minimization of the discharge coefficient to control the normal leakage flow component. A detailed numerical study of rotor-tip winglets, using a two-dimensional (2-D) turbulent flow formulation in primitive variables, is reported. Long and short winglets on the pressure, suction, and both sides (partial shroud) of the blade tip are analyzed. The results of the viscous analysis indicate superior performance with a partial shroud. The numerical technique is extended further to incorporate the axial flow effects by solving the full three-dimensional (3-D) Navier-Stokes equations with tip clearance effects included in the analysis. The 3-D model is validated by comparing it with the experimental results of the double-sided discharge rig of an earlier investigation. In addition, the variations in the specification of the boundary conditions at the inlet and exit of the pressure and suction side channels are investigated in detail. Comparison of the numerical and experimental results suggests an improvement in the predictive capability of the 3-D model over the 2-D analysis.

Nomenclature

b = height of the channel
C_D = discharge coefficient
$C_{D_{2D}}$ = discharge coefficient for 2-D model (Ref. 9)
D = dilation term $\left(\frac{\partial u}{\partial x}+\frac{\partial v}{\partial y}+\frac{\partial w}{\partial z}\right)$
L_c = axial length of tip clearance slot (3-D model)
L_d = axial length of blade downstream of tip clearance (3-D model)
Lg = tip clearance, gap height (3-D model)
L_p = width of pressure side channel (3-D model)
L_s = width of suction side channel (3-D model)
L_u = axial length of blade upstream of slot (3-D model)
ℓ_w = length of winglet
p = normalized static pressure
Δp = pressure drop
q = u,v,w
R = Reynolds number
t = time
t_w = thickness of winglet
t/τ = blade tip thickness/tip clearance at midchord
u,v,w = x,y,z components of velocity
W_∞ = upstream velocity in the pressure side channel
x,y,z = Cartesian coordinates
τ = tip clearance (2-D model)
ρ = density
∇ = gradient (del operator)
ν = kinematic viscosity

Subscripts

FLAT = flat tip, baseline
IN = inlet condition
GAP = tip clearance
i,j,k = node indexes in x,y,z directions

Presented as Paper 83-1171 at the AIAA/SAE/ASME 19th Joint Propulsion Conference, Seattle, Wash., June 27-29, 1983; received July 9, 1983; revision received May 3, 1984.

*Senior Project Engineer, Heat Transfer, Allison Gas Turbine Operations; presently with General Electric Company, Evendale, Ohio.

I. Introduction

THE continuing trend in aircraft gas turbine engines toward higher stage loading and lower aspect ratios[1] has caused secondary flows and mixing effects to have increased importance. Endwall losses constitute a major portion of the total losses, and a significant proportion of the total endwall flow losses is attributed to tip leakage flow. Several models have been proposed to predict blade tip gap effects in turbomachines. The semitheoretical model for predicting the loss in compressor efficiency due to the presence of tip clearance developed by Lakshminarayana[2] is based on the cascade data of Lakshminarayana and Horlock.[3,4] The model developed by Smith[5] is based on measurements with the General Electric multistage low-speed compressor, and Koch and Smith[6] simplified this model to establish the design point efficiency of multistage compressors. Further modifications to the model[5] were made by Adkins and Smith[7] to account for the spanwise influence of tip clearance.

Using a water table and a series of simple geometries, Booth et al.[8] examined the flow across a tip gap (single- and double-sided discharge rigs) without relative wall motion. They identified three major regions in which different terms of the momentum equation are dominant. The tests showed tip leakage flow to be primarily inviscid, and that viscous effects were reduced to creating separations and reattachments. It was determined that the rotor tip could be modeled as a special orifice, and that even though streamwise momentum becomes nearly uncoupled during the leakage process, it is preserved across the gap. Wadia and Booth[9] computed the two-dimensional (2-D) streamline patterns in the tip region, illustrating circulation above the suction surface adjacent to the tip region. They also showed that, for a turbine, discharge coefficients were reduced due to wall motion because the relative movement of the wall was against that preferred by the leakage flow. Several tip configurations were analyzed and the pressure side winglet was found to seal quite effectively.

The objectives of this paper are twofold. Since rotor-tip winglets have been proven to represent good sealing configurations[8-10] the need for further investigation, using the design optimization technique similar to that of Wadia and Booth,[9] becomes evident. The sealing effects, in the form of a discharge coefficient for long and short winglets on the pressure, suction, and both sides (partial shroud) of the blade tip are analyzed to determine 1) whether the pressure side winglet seals better than the suction side winglet, 2) winglet

geometric effects on leakage flow, and 3) the cumulative effect of the pressure and suction side winglets on a partial shroud configuration.

While the 2-D analysis[9] can perform remarkably well to study tip treatment (winglets, grooves, etc.) effects, any form of shroud (casing) treatments, excluding possibly radial grooves, is beyond the scope of the 2-D theory. In addition, while the 2-D viscous flow model is capable of predicting the effects due to relative tangential wall motion, the axial component of wall motion cannot be simulated. Although the analysis is very useful in discerning the qualitative effects of viscosity and wall motion on tip leakage flow, its applicability is limited since it does not provide the leakage flow due to blade unloading or chordwise variation of the leakage velocity.

Due to the limitations of the 2-D simulation of tip leakage flows, this investigation also reports on the development of a three-dimensional (3-D) viscous flow model using the Navier-Stokes equations. The results obtained by the numerical method are compared with the experimental data obtained on the double-sided discharge rig.[8] The 3-D results are also compared with those of the 2-D theory, and it is found that the inclusion of axial (streamwise) effects on tip leakage flow (3-D model) predicts the discharge coefficient more accurately than the 2-D analysis.

II. Background of the Flow Rigs

To support the leakage flow analyses developed by Booth et al.[8] and Wadia and Booth,[9] a series of simple tests was conducted on several flow rigs to actually measure leakage amounts over a *simulated* blade tip. All the tests were conducted in water. Two of the water rigs used for the tests are shown schematically in Figs. 1 and 2, in which the fundamental measured quantities are gap leakage flow and pressure.

The first test rig, shown in Fig. 1, represents the single-sided discharge rig, which was used[8] to measure the impact on tip leakage of pressure side transverse-flow velocity, gap pressure ratio, and gap clearance height.

The effects of the suction side transverse velocity were not measured in the single-sided discharge rig. A new water rig, designated the double-sided discharge rig (shown in Fig. 2), was designed to simulate this effect. This rig produced transverse flows on both the pressure and suction sides of the tip clearance space. The transverse velocity and pressure levels of each stream could be varied independently through four pinch valves. Further details of the single- and double-sided discharge rigs are reported in Refs. 8 and 9.

The design optimization of the winglets described in the following sections is based on the analysis developed using the single-sided discharge rig, while the 3-D viscous analysis is developed and validated using the experimental data obtained on the double-sided discharge rig.

III. Design Optimization of Rotor-Tip Winglets

The endwall inviscid iterative leakage algorithm developed by Booth et al.[8] and Okapuu and Moustapha[11] was used to calculate the leakage flow at each chordwise station parallel to the leakage paths. Knowing the leakage paths, the decoupling principle, whereby streamwise momentum becomes nearly uncoupled during the leakage process, was applied to the design of new flow-control configurations as a part of a component improvement program (CIP). The numerical method used to calculate the viscous flow through the specially modeled orifices was a minor modification of the TEACH code[12] developed at Imperial College. The basic forms of the boundary conditions along the shroud endwall and the blade walls and along the inflow and outflow boundaries were similar to those of Wadia and Booth.[9]

An extensive series of numerical calculations was conducted using the design optimization viscous code applied to the leakage flow orifices in the neighborhood of the midchord region of the blade tip at a gap Reynolds number of 6000. Altogether, seven different configurations were analyzed. The configurations represented variations of the recently developed turbine concept of a "winglet." The configurations analyzed are shown in Fig. 3. The inlet turbulence level in the analysis was less than 1%.

The selection of the midchord region for the 2-D viscous analysis was based on the experimentally observed relative velocity vectors inside the tip clearance region of a compressor rotor of Pandya and Lakshminarayana.[13] In their experiments, Pandya and Lakshminarayana noted that, at approximately 50% chord length, the flow turned abruptly in the tangential direction, giving rise to a substantial leakage velocity. Downstream of the midchord section, the leakage flow was predominant. In addition, the winglets generally are the longest between 35%-65% chord length, giving rise to substantial viscous effects and consequently separations and reattachments.

The fundamental idea behind the winglet design (Fig. 3b) was to produce a large inlet pressure drop by having the flow come down from the hub to the tip over the sharp edge, with the probability of even greater improvement by reducing the surface-to-surface pressure drop with actual airfoils. The rationale behind longer pressure and suction side winglets (Figs. 3c and 3e) was to have a longer surface for the tip leakage flow, which would induce more boundary layer blockage effects due to the viscous nature of the flow within the modeled orifice.

The results of the viscous analysis using the TEACH code are shown in Fig. 4. The short pressure side winglet (Fig. 3b)

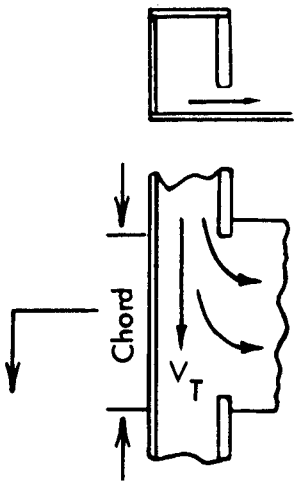

Fig. 1 Single-sided discharge rig.[8,9]

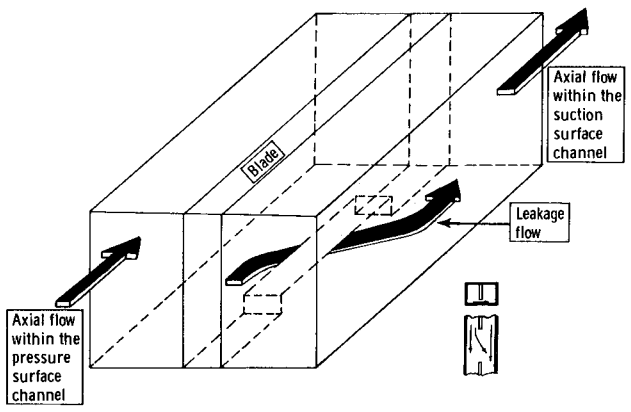

Fig. 2 Schematic of the double-sided discharge rig.[8]

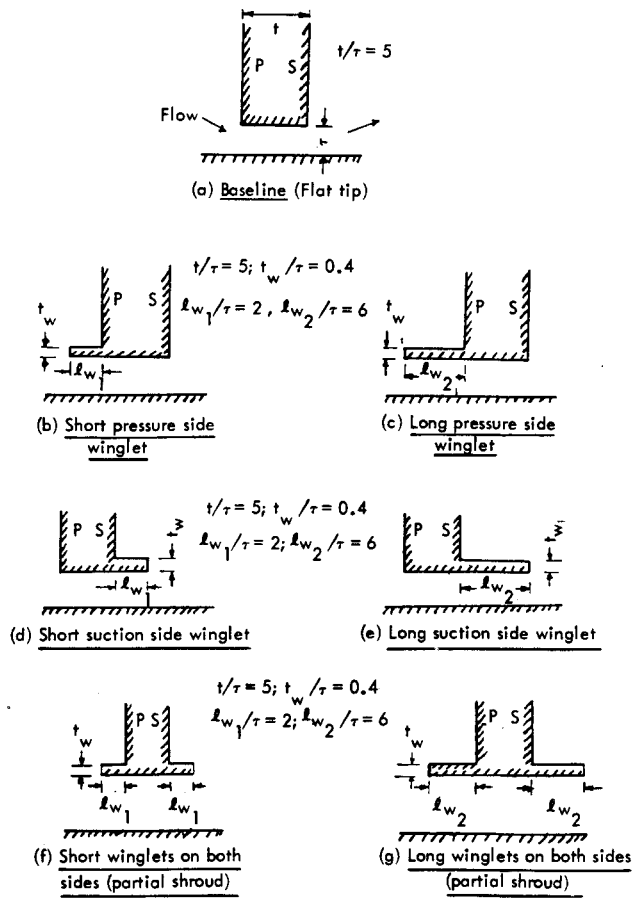

Fig. 3 Rotor-tip winglet configurations analyzed.

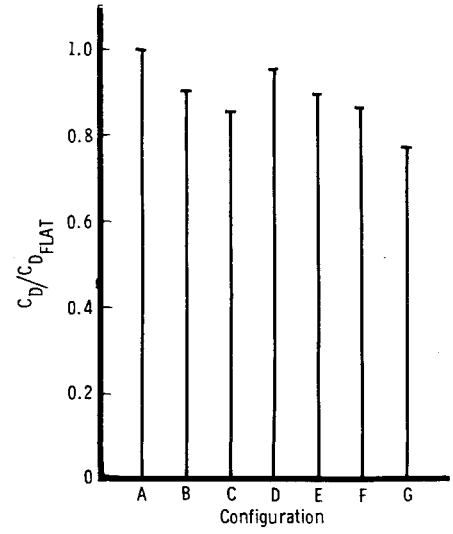

Fig. 4 Sealing effectiveness ranking for rotor-tip winglet test series.

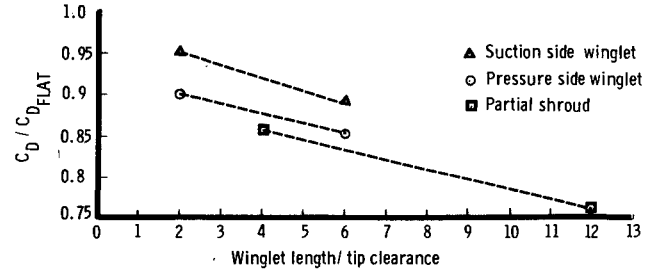

Fig. 5 Distribution of the discharge coefficient with the length of winglet.

produced about a 10% decrease in discharge coefficient, while the short suction side winglet (Fig. 3d) reduced the discharge coefficient by 5% compared with the baseline (Fig. 3a). This indicates the significant effect the inlet blade tip geometry has on leakage flow. Modification of the exit geometry of the blade tip (suction side winglet, Fig. 3d) obviously does affect the roll-up vortex on the suction side, but the reduction in leakage flow is about 50% less than that due to the pressure side winglet (Fig. 3b). Tripling the length of the pressure and suction side winglets (Figs. 3c and 3e) resulted in a reduction in the discharge coefficient that was 5.3% and 6.2% more, respectively, than that of the short pressure and suction side winglets. The short and long partial shroud configurations (Figs. 3f and 3g) resulted in a reduction in C_D of approximately 14% and 24%, respectively, in leakage flow compared with the baseline configuration.

The variation of the discharge coefficient with the ratio of the length of the winglet to tip clearance for the same Reynolds number (based on gap height) is shown in Fig. 5. The viscous analysis indicates that it might be possible to predict the discharge coefficient of a partial shroud (total winglet length $= \ell_{w\ ps} + \ell_{w\ ss}$) by taking the product of the discharge coefficients of the pressure side winglet (length of winglet $= \ell_{w\ ps}$) and the suction side winglet (length of winglet $= \ell_{w\ ss}$). In addition, Fig. 5 illustrates that for the same length of winglet, the partial shroud is a better sealing configuration than the pressure side winglet.

The variation of the discharge coefficient with the ratio of the winglet thickness (t_w) to the total length of the blade tip orifice model ($t + \ell_w$) is shown in Fig. 6. The results show reduction in discharge coefficient with decreasing winglet thickness, which is consistent with the results of the laminar flow analysis.[9]

To summarize, a series of calculations employing the viscous flow design code was conducted to demonstrate the sealing performance of several different winglet configurations. The numerical calculations, which are qualitatively in excellent agreement with the experimental studies on the water rigs,[8,9] showed that winglets could be ranked in the following order of deteriorating leakage performance: 1) partial shroud, 2) pressure side winglet, and 3) suction side winglet.

Moreover, it appears that the product of the discharge coefficients for the pressure and suction side winglets results in the discharge coefficient for a partial shroud configuration.

IV. Three-Dimensional Viscous Flow Analysis

Governing Equations

The time-dependent 3-D laminar viscous flow equation for incompressible fluids is:

$$\frac{\partial q}{\partial t} + q \times \nabla q = -\nabla p + \frac{1}{R}\nabla^2 q \tag{1}$$

and the Poisson equation for pressure is:

$$\nabla^2 p = \frac{1}{R}(\nabla^2 D) - \left(\frac{\partial^2(u^2)}{\partial x^2} + \frac{\partial^2(v^2)}{\partial y^2} + \frac{\partial^2(w^2)}{\partial z^2} + 2\frac{\partial^2(uv)}{\partial x \partial y} + 2\frac{\partial^2(vw)}{\partial y \partial z} + 2\frac{\partial^2(uw)}{\partial x \partial z} + \frac{\partial D}{\partial t}\right) \tag{2}$$

In the above equations, distance was normalized by the tip clearance time by the advective constant (Lg/W_∞), velocity by the inflow freestream axial velocity on the pressure side, and pressure by the dynamic pressure (ρW_∞^2). The Reynolds

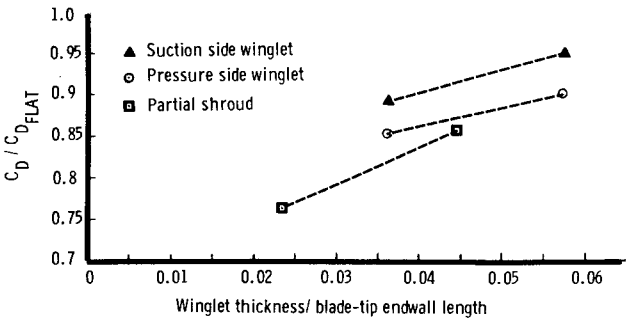

Fig. 6 Variation of the discharge coefficient with the thickness to blade tip endwall length ratio.

number is based on the tip clearance and the pressure side axial flow velocity.

Table I in Ref. 8 illustrates four types of driving mechanisms associated with rotor tip leakage flows in an engine. They are: 1) pressure side transverse flow, 2) suction side transverse flow, 3) streamwise pressure distribution, and 4) moving endwalls. The model selected for the verification of three-dimensional analysis (Fig. 2) satisfies the transverse flow requirements of real blade geometries and moving endwalls can be incorporated easily by appropriately changing the no-slip condition on the shroud. The limitations of the present model are: 1) its inability to generate true streamwise pressure distribution unless curved channels are used with an orthogonal grid system, and 2) zero clearance levels upstream of the leading edge and downstream of the trailing edge.

In Eq. (1), x is the blade-to-blade direction, y varies from hub to tip, and z is the direction of axial flow.

Finite Difference Approximation

The finite difference scheme for the momentum equations basically consisted of a forward difference approximation for the time derivative, upwind differencing for the convective terms (similar to Ref. 9), and central differencing for the pressure and viscous terms. Nonuniform grid spacing was used in all three directions, with a dense mesh within the tip clearance space and at all no-slip surfaces. Numerical experiments indicated the necessity for more mesh points near the leading and trailing edges of the tip gap and at all sharp corners. Upstream of the blade tip gap (Fig. 2), a coarse mesh was used.

Following Harlow and Welch,[14] the time derivative $\partial D/\partial t$ is evaluated by explicit first-order accurate time differencing, such that

$$\frac{\partial D}{\partial t} = -\frac{D^n_{i,j,k}}{\Delta t} \tag{3}$$

Neumann conditions for the pressure equation require special formulation in the incorporation of the gradient condition in the successive-over-relaxation method. The method recommended by Miyakoda[15] was used to produce convergent solutions. The derivative boundary conditions were incorporated directly into the discretized equations at interior points adjacent to the boundaries. Thus, the standard finite difference approximation of the Poisson equation for Eq. (2) was used only at interior points that were more than one node removed from the boundaries. At points adjacent to a boundary, the derivative conditions are incorporated directly into the relaxation scheme, and the pressure gradients are computed using the second order accurate finite difference approximation of the momentum equations. After convergence, the final boundary values of pressure are computed using second order Taylor's series expansion of the pressure gradients.

The second special formulation for Neumann conditions is that the boundary gradients should be compatible with the source term. By following guidelines similar to Miyakoda, $\partial p/\partial n$ was computed to second-order accuracy to meet this constraint.

The procedure just described appears to be well suited for the solution of the Poisson equation for pressure to solve the tip leakage problem. The specification of Dirichlet boundary conditions for pressure at the inlet (and when possible at the exit) tends to accelerate the overall convergence of the method.

The large machine time required to solve the discretized form of the governing equations of motion were significantly reduced by decreasing the number of grid points within the endwall boundary layers. The justification for this is based on the experimental observation[8] that tip leakage flow is primarily an inviscid, pressure driven phenomenon and viscous effects are of second order. The areas affected most predominantly as a consequence of this assumption lie in the vicinity of the leading and trailing edges of the leakage slot.

Boundary Conditions

The present work involved the development of realistic, accurate, and stable boundary conditions for the blade tip leakage flow analysis.

Along the shroud endwall and the blade walls, the boundary conditions specified are no-slip, thus allowing specification of tip speed through a relative wall translation. At the upstream surface in the pressure and suction side channels, the axial components of velocity were specified with $u = v = 0$. At the exit of the flowfield, downstream of the tip gap, the normal components of the velocity gradients were specified as zero.

The pressure was specified at the inlet in both the channels. Though the numerical problem can be solved with all specified Neumann boundary conditions for pressure, numerical experiments showed that the specification that just the axial velocity on the pressure side is more than that on the suction side is not sufficient to determine the direction of the leakage velocity from the pressure side to the suction side of the blade. The imposition of the inlet pressures was found to represent the physically meaningful leakage flow mode suitably.

The rest of the boundary conditions of the Poisson equation of the pressure field were of the second kind, specifying $\partial p/\partial n$ where n is the normal to the boundary. The boundary-layer assumption that $\partial p/\partial n = 0$ was not made, and the gradients were calculated from the momentum equations. For transient solutions, the time-dependent terms in the momentum equations were neglected.

For the double-sided discharge rig,[8] the flow was metered by four orifices, two of which were downstream of the tip gap. Metering of the downstream flow implies an a priori specification of the leakage flow, which leads to the specification of the boundary conditions for pressure at the exit of both the channels in the numerical model. The results of the experiment are compared with the numerical calculations in the latter portions of this paper.

Near the sharp corners in the tip clearance region, the use of Neumann boundary conditions results in a double-valued pressure. Although this is nonphysical, the double value was retained, as in the method for the discontinuous treatment for a double-valued vorticity.[9] Numerical experiments suggest the largest errors due to such a treatment occur in the vicinity of the corners where the flow either contracts or expands suddenly, especially near the leading edge of the tip gap on the pressure side. These effects appear to have been reduced downstream of the inlet to the tip clearance space.

Discharge Coefficient

For a specified inlet mass flow and the pressure drop across the blade tip, a discharge coefficient for the 3-D analysis was defined in a manner similar to the double-sided discharge rig

experiment[8] as

$$C_{D_{3D}} = V_{\text{actual}} / V_{\text{frictionless}} \tag{4}$$

where V_{actual} is the measured velocity of the fluid crossing the gap, and $V_{\text{frictionless}}$ is the velocity of the fluid as would be predicted by using the frictionless Bernoulli equation. The frictionless velocity is computed by

$$V^2_{\text{frictionless}} = V^2_{\text{IN}} + 2\Delta p \tag{5}$$

where V_{IN} is the freestream velocity in the high-pressure channel and Δp is the average pressure drop across the ends of the clearance gap. The actual gap velocity is given by

$$V^2_{\text{actual}} = V^2_{\text{IN}} + V^2_{\text{GAP}} \tag{6}$$

where V_{GAP} is an average of the crosswise component of the fluid velocity in the clearance space.

The discharge coefficient for the 2-D analysis for comparisons with the 3-D calculations is similar to that defined by Wadia and Booth.

V. Numerical Results

Three different cases were tested using the 3-D numerical method described in this investigation. Two of the cases were geometrically similar, but the forms of the boundary conditions for pressure were different. The three cases will be henceforth referred to as cases A, B, and C.

Case A

The test section height and width were 1.016 and 1.106 cm, respectively, and the flow area was 1.032 cm^2. The axial slot length, blade thickness, and tip clearance were 1.016, 0.508, and 0.254 cm, respectively.

The Reynolds number, based on tip clearance, was 1000 and the inlet freestream velocity on the pressure side was 40.2 cm/s. The ratio of the inlet pressures on pressure and suction sides was 1.266. The downstream boundary conditions for pressure were of the second kind.

Case B

This case represents an actual scaled water rig test conducted in conjunction with the Low Aspect Ratio Technology program, and the geometric and flow conditions are specified in Ref. 8. Because control was exercised over both the inlet and exit through four pinch valves in the experiment, the inlet and exit pressures were specified in the analysis, resulting in a much faster convergence of the numerical technique.

Case C

Case C is exactly similar in geometry to case B, except, in the analysis, the exit pressure boundary condition was relaxed, and the gradient condition on pressure was imposed at all outflow boundaries. This was analyzed to demonstrate the significance of the downstream boundary condition on leakage flow.

Velocity Vector Plots

Figure 7 shows the velocity vectors in the x-z plane at four different radial locations within the tip clearance and two radial locations above the tip gap for case A.

At all radial locations within the tip clearance space, a distinct separation region can be seen at the leading edge of the axial slot. The axial and tangential components of velocity increase downstream of the leading edge of the model. The flow begins to turn in the tangential direction at the midchord region, with substantial leakage velocity between 75% and 100% of the axial slot length, which is consistent with the qualitative trends of Pandya and Lakshminarayana's[13] experiments. In an actual engine environment, flow reversal at the leading edge will not occur; however, the tangential component of the leakage velocity will be negligible compared with the axial velocity component. Beyond 50% of the axial slot length, a large change in the flow angle occurs from the pressure surface to the suction surface, indicating an extremely active region of leakage flow.

The axial component of velocity in the pressure side channel is turned in the tangential direction toward the axial slot from approximately the midwidth location. The flow in the pressure side channel downstream of the tip clearance region is almost axial in nature.

The axial velocity in the suction side channel does not appear to be affected significantly by leakage flow until the midlength of the axial slot, where the leakage begins to dominate the flow in the channel. The flow is almost tangential in the suction side channel at the trailing edge of the tip gap. Downstream of the slot, the axial and tangential components of velocity in the region near the blade wall are very small until the leakage flow is turned in the axial direction at the midwidth of the suction side channel.

The through-flow in both the pressure and suction side channels is not significantly affected by leakage flow beyond the midwidth region of each channel. The effect of the leakage flow within the tip clearance region is also felt above the tip gap region, as shown in Fig. 7f. This effect is reduced in the vicinity of the hub section of the blade.

Figure 8 shows some of the corresponding velocity vectors in the x-y plane at different axial stations along the tip clearance slot. In the figure, z is measured from the leading edge of the tip clearance slot. Figures 8a-8c show the velocity vectors within the tip clearance space and the development of the tip votex (Appendix) on the suction side of the blade. The flow has a tendency to migrate from hub to tip in the blade wall region on the pressure side. The figures illustrate that the tip flow downstream of the slot leading edge forms a thin jet that streams out into the main flow (on the suction side), maintaining its identity until it is rolled up into a tip vortex by the main flow. The tangential component of velocity as the flow enters the tip clearance space near the leading-edge region of the slot is larger in magnitude on the pressure side than on the suction side and vice versa near the trailing edge of the tip gap.

Figure 8d shows the roll-up vortex decaying as it propagates downstream of the axial slot. The tangential velocity component in the pressure side channel downstream of the slot is negligible. The leakage velocity at the trailing edge is larger than the velocities at all the other axial locations due to the formation of the leakage vortex and the subsequent entrainment by the vortex. In general, a vena contracta effect is visible as the flow rounds the corner from the pressure side into the tip gap. The tangential velocity is larger in the vicinity of the shroud relative to the blade tip region. At the exit of the slot (near the suction side of the blade), the tangential velocity near the blade tip is larger than that in the neighborhood of the endwall. The velocity vector plots shown in Fig. 7 tend to confirm that near the blade tip region, the inflow and outflow boundaries can be realistically modeled to simulate the physical phenomenon accurately, with a radial potential flow solution for a 2-D design optimization analysis.[9]

Pressure Distribution

The normalized static pressure distribution within the tip clearance space at several axial locations is illustrated in Fig. 9. The distribution is qualitatively similar to the measurements of Wadia and Booth.[9] The results indicate that the largest pressure drop occurs as the flow enters the tip gap and that a small recovery is made as the flow exits on the suction side, which is in good agreement with the prior[9] measurements.

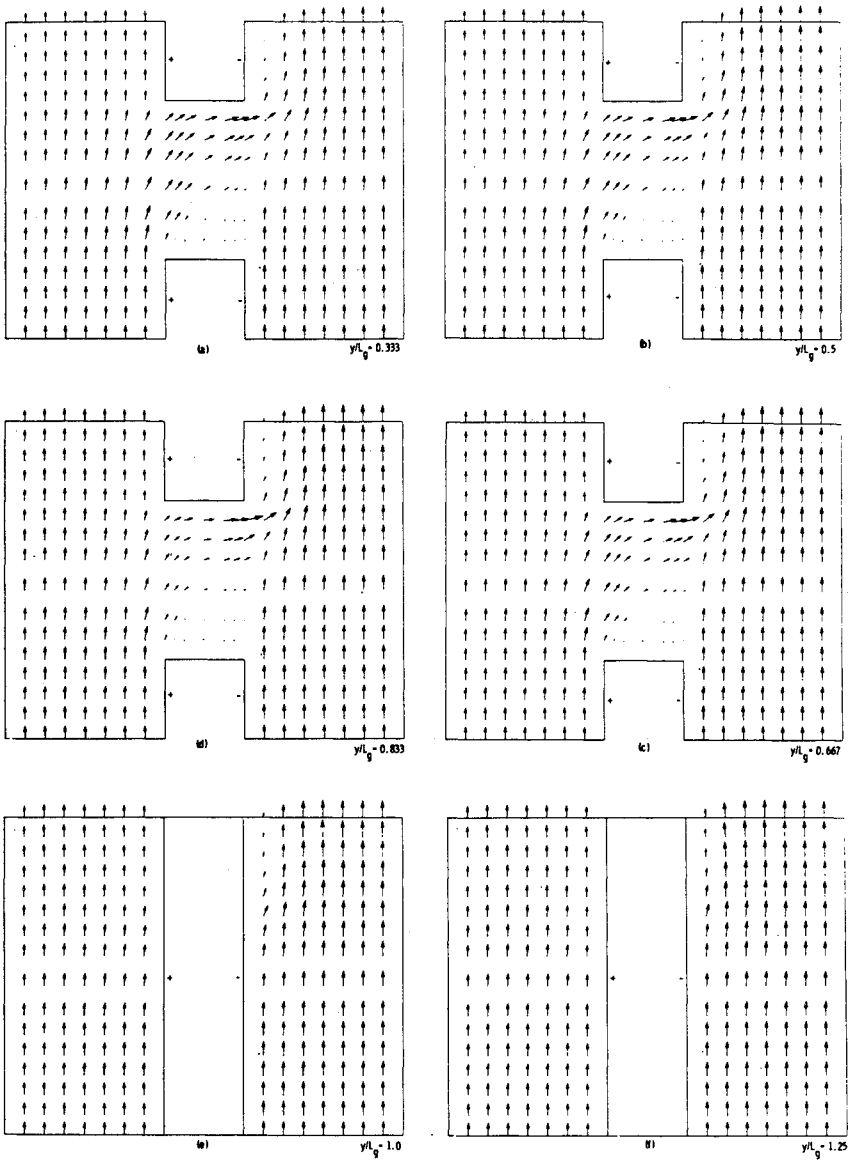

Fig. 7 Velocity vectors in the x-z plane inside and above the clearance region at different radial locations.

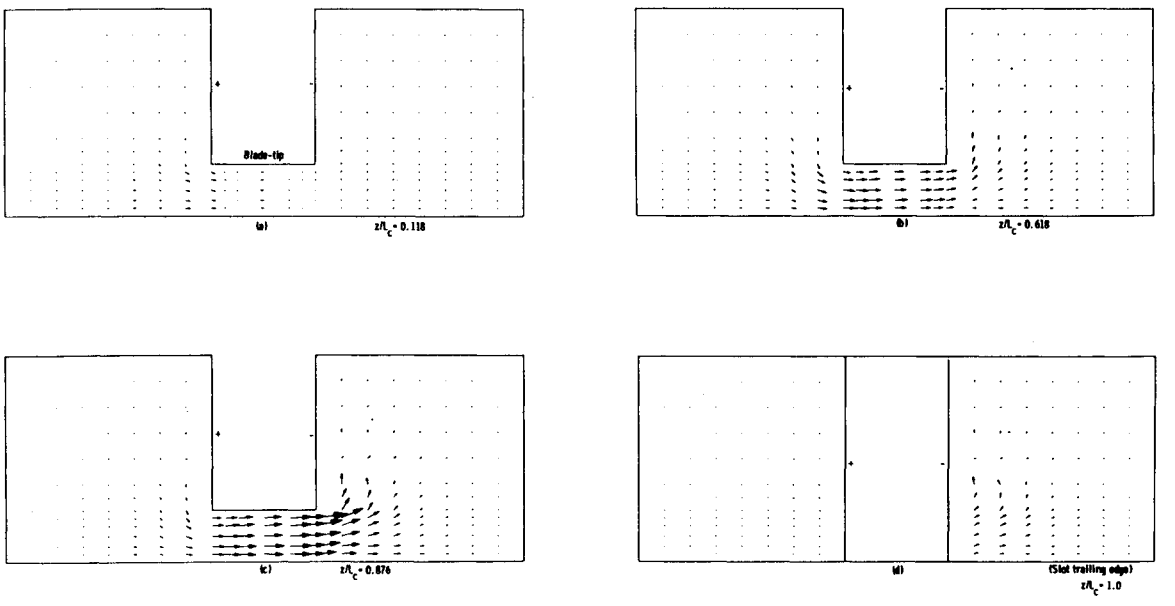

Fig. 8 Velocity vector in the plane normal to the camber line.

Crosswise Velocity Profile

The local tangential velocity distribution within the gap at several axial locations is shown in Fig. 10. The cross-flow velocities indicate that the maximum leakage flow occurs in the downstream half of the axial slot, as stated earlier. The velocity profiles appear to indicate that the endwall boundary layer is extremely thin in the downstream slot region, which is most probably due to the strong jet discharging into the suction side channel. The velocity profiles tend to be very flat, and there appears to be a shear layer present in the vicinity of the endwall and the blade tip.

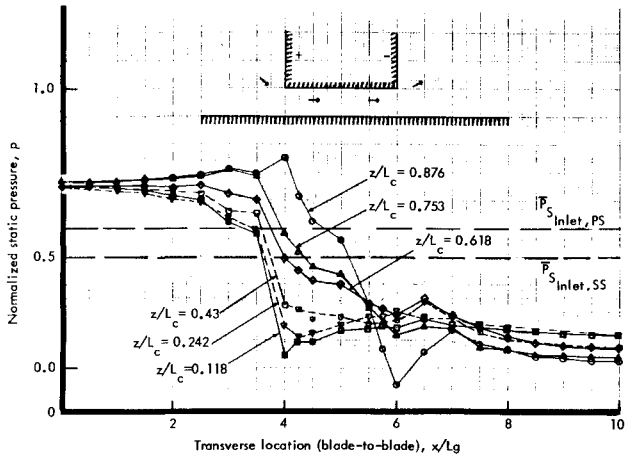

Fig. 9 Variation of the static pressure across the blade tip ($y/Lg = 0.5$).

Discharge Coefficients

Table 1 summarizes the test results in terms of the discharge coefficients for cases A, B, and C described previously.

Table 1 shows the improvement in the prediction of the discharge coefficient using the 3-D viscous flow model vs the 2-D analysis for case B. It also illustrates that the decoupling principle developed in Ref. 8 and applied in Ref. 9 is based on sound principles of basic fluid mechanics and is realistic and physically meaningful, and that the 2-D approach (neglecting axial flow effects) can be successfully used in optimization studies of tip leakage flows.

The throttling effect at the exit boundary in the numerical solution has a significant effect on leakage flow at the upstream stations, as demonstrated by comparing the discharge coefficients for cases B and C. Case B indirectly reflects on a prespecified leakage flow due to the specification of the exit boundary conditions on pressure in both the channels, which subsequently sets up the pressure drop across the clearance space.

Comparison with Experiment

Figure 11 shows the comparison of the static pressure distribution between the experiment[8] and the present 3-D

Table 1 Comparison of discharge coefficients with other experiments

Case	Present 3-D model	2-D analysis[9]	$C_{D_{EXPT}}$[8]
A	0.7593	—	—
B	0.8148	0.7812	0.821
C	0.9262	—	—

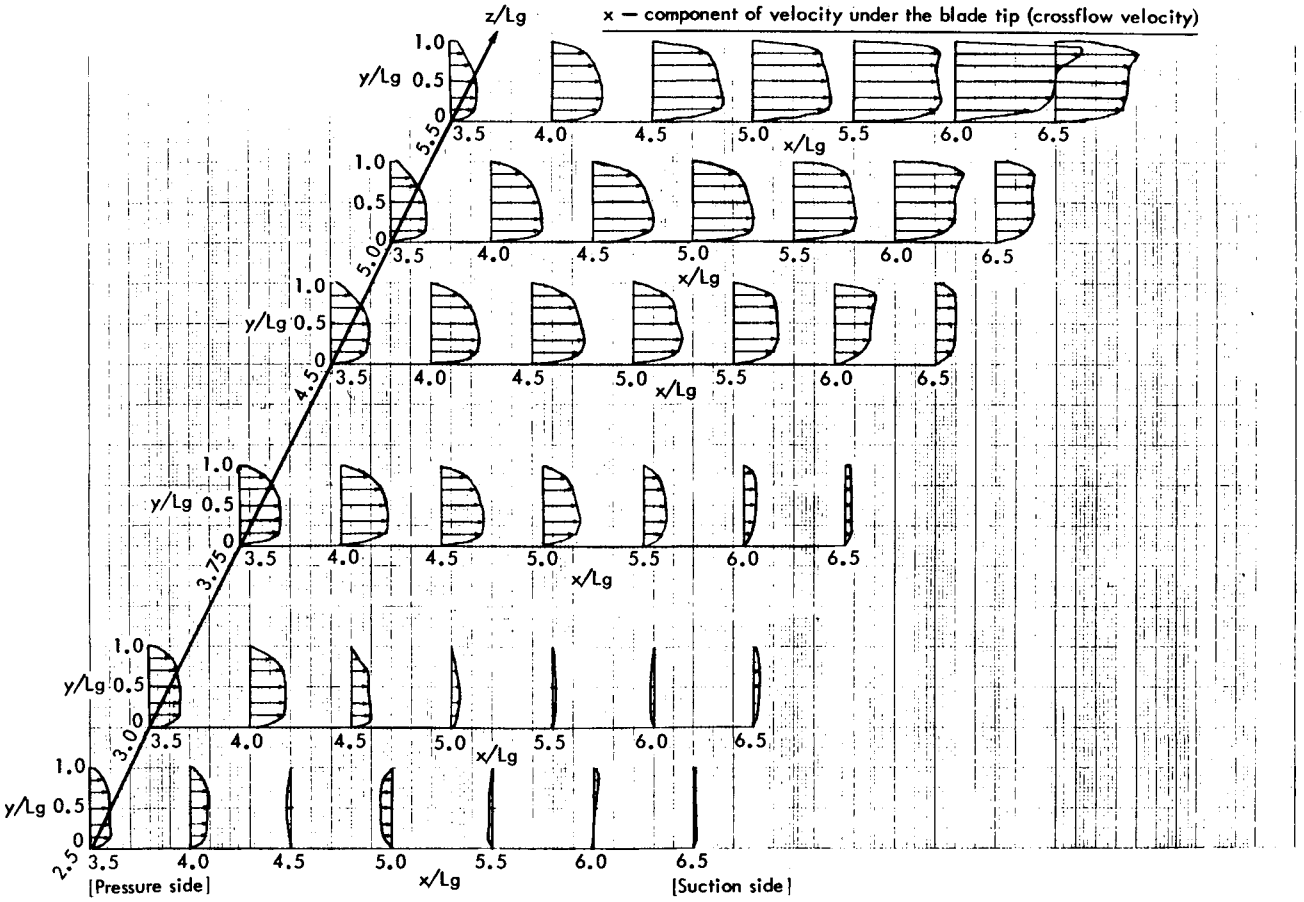

Fig. 10 The x component (tangential) of velocity under the blade tip at different axial locations.

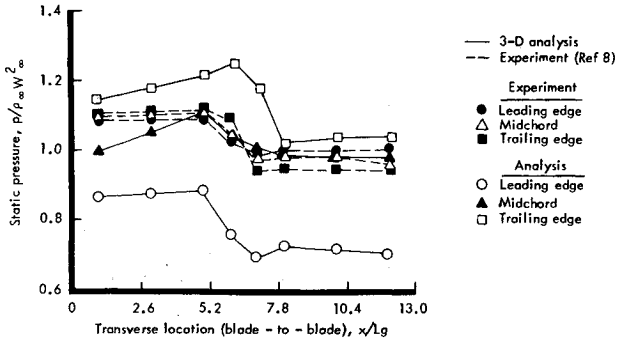

Fig. 11 Comparison of the static pressure distribution for case B.

analysis for case B. The results show reasonably good agreement with experiments at 50% chord. The numerical method tends to underestimate the pressure at the leading edge and overestimate the pressure at the trailing edge of the axial slot. The discrepancy in the results at the leading and trailing edges is most probably due to the numerical errors associated with corner modeling of the pressure term and grid resolution. The other source of error might be false diffusion effects caused by upwind differencing of the convection terms wherein the flow might tend to anticipate the corners and consequently adjust the upstream flow conditions inaccurately.

To summarize, the numerical method proposed here appears to be well suited for the analysis of tip leakage flows in turbomachines. The analysis suggests that the major portions of the leakage flow occur between 50% chord and the trailing-edge region. The results indicate that the shroud-leakage algorithm[8] coupled to the 2-D viscous code[9] can be useful in the design optimization of leakage flows.

VI. Conclusions

The objectives of the tip leakage investigation were twofold: 1) further improvements in rotor-tip winglet configurations were needed using the systematic and economical approach developed in Ref. 9, and 2) an adequate model, directly compatible with a 3-D viscous solution or a stand-alone full rotor analysis, was required.

The first objective resulted in the following answer to an important question raised by many turbine designers: the pressure side winglet is a more effective sealing configuration than a suction side winglet. The numerical results suggest that a partial shroud is the best performer among all the members of the winglet family. This has also been supported by some earlier water table experiments.[8]

The second objective was achieved by developing a full 3-D viscous flow model of the tip leakage problem capable of incorporating arbitrary wall motion to account for blade rotation. Because of the complexity of 3-D leak processes, only one configuration (i.e., flat tip) was analyzed in detail. The solution indicates that most of the leakage flow occurs beyond 50% chord. The presence and interaction of tip leakage flow and annulus wall boundary layer are the most dominant features from the midchord to the trailing-edge regions of the axial slot. As observed in Ref. 9, for a turbine, discharge coefficients will be reduced due to wall motion, because the relative tangential movement of the wall is against that preferred by the leakage flow.

The leakage flow rolls up into a tip vortex approximately halfway between the blade passage on the suction side, and the tip vortex propagates downstream beyond the region of the axial slot. The axial velocity component increases as the flow leaves the suction side channel. Leakage velocity computations show that it is very small at the entrance of the tip clearance space and increases significantly downstream of the midchord region. The leakage velocity is the maximum at the trailing edge of the tip clearance space.

The modeling for the 3-D analysis was developed within a simplified framework. Simplifying elements included two rectangular channels, laminar flow, and an axial slot. These simplifications were made consistent with the ability to verify the details of the solution based on the water table experiments.

The current analysis is now properly viewed as an accurate starting point for the development of a more detailed full-rotor analysis. Modifications and superposition of blade wall pressures from 2-D cascade analysis can incorporate the effects of blade curvature in the solution. Further refinements would include arbitrary wall motion, supplying an appropriate turbulence model, and introducing compressibility and tip coolant injection. The simplified geometry can be used effectively to study advanced tip configuration concepts for turbine rotors or new shroud configurations (e.g., grooves, axially skewed slots, etc.) for surge-to-stall margin improvements in axial compressors. The availability of the tip solution presented here has provided the means to design high performance blade tips that retain effective sealing at higher clearance levels.

Appendix: Extraction of the Vortex Structure in the Plane Normal to the Camber Line

For the purpose of better flow visualization and qualitative comparison with the two-dimensional streamline patterns,[9] the vortex structure in the plane normal to the camber line can be extracted from the three-dimensional results in the following manner. The governing equation of the flow normal to the camber line (i.e., decoupling the x-y plane from the x-y-z domain) in stream function-vorticity formulation is

$$\nabla^2 \psi_z = -\omega_z \tag{A1}$$

where the vorticity ω_z and the stream function ψ_z are defined as

$$\omega_z = \frac{\partial v}{\partial x} - \frac{\partial u}{\partial y} \qquad u = \frac{\partial \psi_z}{\partial y} \qquad v = -\frac{\partial \psi_z}{\partial x} \tag{A2}$$

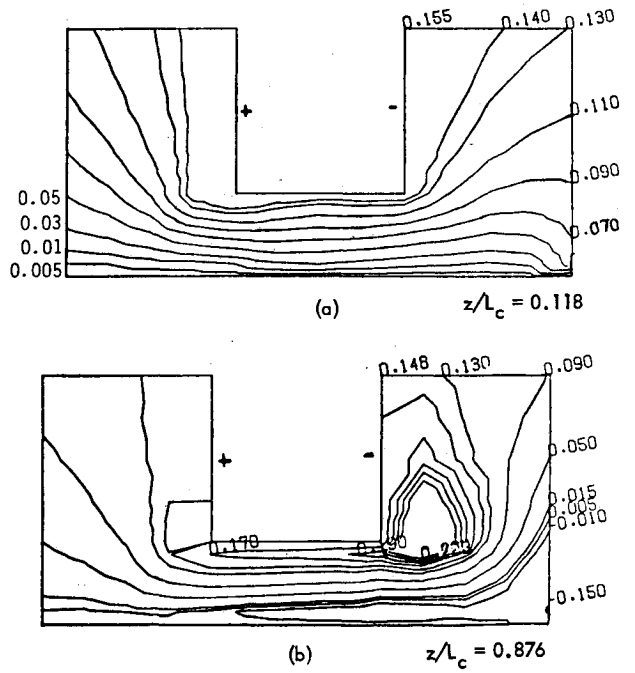

Fig. A1 Computer generated streamlines showing the tip vortex formation.

The values of the source term, ω_z, in the Poisson equation (A1) and the stream function at all boundaries in the x-y plane are calculated a priori from the known values of u and v obtained by the 3-D analysis. The Poisson equation (A1) is then solved by the successive over-relaxation method. The streamline patterns in the vicinity of the blade-tip at two axial locations are shown in Fig. A1. The suction side tip vortex thus obtained is qualitatively similar to that of the two-dimensional calculations.[9] In addition, separation near the pressure side wall at the blade-tip was also observed.

References

[1]Liu, H. C., Booth, T. C., and Tall, W. A., "An Application of 3-D Viscous Flow Analysis to the Design of Low Aspect Ratio Turbine," ASME Paper 79-GT-53, 1979.

[2]Lakshminarayana, B., "Method of Predicting the Tip Clearance Effects in Axial Flow Turbomachinery," *ASME Journal of Basic Engineering*, Vol. 92, 1970, pp. 467-482.

[3]Lakshminarayana, B. and Horlock, J. H., "Tip Clearance Flow and Losses for an Isolated Compressor Blade," Aeronautical Research Council, R&M 3316, 1963.

[4]Lakshminarayana, B. and Horlock, J. H., "Leakage and Secondary Flows in Compressor Cascades," Aeronautical Research Council, R&M 3483, 1967.

[5]Smith, L. H. Jr., "Casing Boundary Layers in Multi-Stage Axial Flow Compressors," *Proceedings of the Symposium on Blading-Flow Research on Blading*, edited by L. Z. Dzung, Elsevier Publishing Co., Amsterdam, 1970.

[6]Koch, C. C. and Smith, L. H. Jr., "Loss Sources and Magnitudes in Axial Flow Compressors," *ASME Journal of Engineering for Power*, Vol. 98, July 1976, pp. 411-424.

[7]Adkins, G. G. Jr. and Smith, L. H., "Spanwise Mixing in Axial-Flow Turbomachines," *ASME Journal of Engineering for Power*, Vol. 102, 1982, pp. 97-110.

[8]Booth, T. C., Dodge, P. R., and Hepworth, H. K., "Rotor-Tip Leakage: Part I—Basic Methodology," *ASME Journal of Engineering for Power*, Vol. 104, Jan. 1982, pp. 154-161.

[9]Wadia, A. R. and Booth, T. C., "Rotor-Tip Leakage: Part II—Design Optimization Through Viscous Analysis and Experiment," *ASME Journal of Engineering for Power*, Vol. 104, Jan. 1982, pp. 162-169.

[10]Patel, K. V., "Research on a High Work Axial Gas Generator Turbine," SAE Paper 800681, Warrendale, Pa., 1980.

[11]Okapuu, U. and Moustapha, S. H., "Discussion—Rotor Tip-Leakage—Part II—Design Optimization Through Viscous Analysis and Experiment," *ASME Journal of Engineering for Power*, Vol. 104, April 1982.

[12]Gosman, A. D. and Pun, W. M., "Calculation of Recirculating Flows," Imperial College, Dept. of Mechanical Engineering, Rept. HTS/73/2, 1973.

[13]Pandya, A. and Lakshminarayana, B., "Investigation of the Tip Clearance Flow Inside and at the Exit of a Compressor Rotor Passage—Part I: Mean Velocity Field," *ASME Journal of Engineering for Power*, Vol. 105, Jan. 1983, pp. 1-12.

[14]Harlow, F. H. and Welch, J. E., "Numerical Calculation of Time-Dependent Viscous Incompressible Flow of Fluid with Free Surface," *Physics of Fluids*, Vol. 8, No. 12, 1965, pp. 2181-2189.

[15]Miyakoda, K., "Contribution to the Numerical Weather Prediction—Computation with Finite Difference," *Japanese Journal of Geophysics*, Vol. 3, 1962, pp. 75-190.